6.3 CERES CLOUD PROPERTY DATABASE FROM VIRS AND MODIS

Sunny Sun-Mack, Yan Chen, Qing Z. Trepte
SAIC, Hampton, VA 23666

Patrick Minnis, Erika Geier
Atmospheric Sciences, NASA Langley Research Center, Hampton, VA 23681

Patrick W. Heck
CIMSS, University of Wisconsin-Madison, Madison, WI, USA

1. INTRODUCTION

The NASA Clouds and Earth's Radiant Energy System (CERES) is providing simultaneous measurement of the radiation and cloud fields on a global basis to improve the understanding and modeling of the interaction between clouds and radiation at the top of the atmosphere, at the surface, and within the atmosphere. CERES Project, begun in 1998, is meeting this need (Wielicki et al. 1998). Broadband shortwave (SW) and longwave radiance measurements taken by the CERES scanners at resolutions between 10 and 20 km on the Tropical Rainfall Measuring Mission (TRMM), *Terra*, and *Aqua* satellites are matched to simultaneous retrievals of cloud height, phase, particle size, water path, and optical depth *OD* from the TRMM Visible Infrared Scanner (VIRS) and the Moderate Resolution Imaging Spectroradiometer (MODIS) on *Terra* and *Aqua*. Besides aiding the interpretation of the broadband radiances, the CERES cloud properties are valuable for understanding cloud variations at a variety of scales. In this paper, the resulting CERES cloud data taken to date are averaged at spatial variability of the cloud properties on a global scale at a 1° resolution and several temporal scales to examine the temporal.

It was demonstrated from earlier studies (Minnis et al. 2002, 2003, 2005) that the CERES cloud property retrievals from *Terra* MODIS, *Aqua* MODIS, and TRMM VIRS were very consistent with the most significant difference being the retrieval of smaller cloud droplet effective radii r_e from the *Terra* data. Comparisons of other parameters with climatological data also showed that the cloud amounts from both TRMM and *Terra* were in good agreement with the zonal means from long-term surface observations and were typically 0.07 - 0.08 less than those from the International Satellite Cloud Climatology Project (ISCCP) dataset (Rossow and Schiffer, 1999) over the Tropics. Comparisons with surface-based retrievals showed that the mean CERES-derived cloud *OD*s for stratus clouds were within 6% of their surface counterparts. These cloud properties have been already been responsible for dramatically improving estimates of the Earth's radiation budget (ERB) by facilitating the most accurate representation of the anisotropy of the radiance fields leaving the Earth-atmosphere system (Loeb at al. 2003). They will also be valuable for linking the hydrological cycle and ERB and for improving cloud processes in climate models. The importance of measuring cloud and radiation changes simultaneously was recently highlighted by measurements of Earth shine that were used to infer a 5 Wm^{-2} increase in the SW flux reflected from the Earth between 2000 and 2003 (Palle et al. 2004). Changes of that magnitude are comparable to those from a major volcanic eruption and should be apparent in the CERES cloud and radiation record and as well as in other measures of the state of the climate. Both the flux and cloud results from CERES do not support the Earthshine conclusions (Weilicki et al., 2005). This paper provides an update on the status of the cloud properties being derived for CERES.

*Corresponding author address: Patrick Minnis, NASA Langley Research Center, MS 420, Hampton, VA 23681-2199. email: p.minnis@nasa.gov.

2. DATA & METHODOLOGY

Aqua has a 1330 LT equatorial crossing and began producing MODIS imagery in early summer 2002. *Terra*, which started producing usable MODIS data in late winter of 2000, nominally crosses the Equator at 1030 LT. The TRMM, launched during late 1997, continues to provide coverage at all local hours between 37°N and 37°S every 46 days. At the time of this writing, *Terra* data have been analyzed to produce the CERES *Terra* Edition 2 Single Scanner Footprint (SSF) dataset through June 2005 and CERES *Aqua* Edition 1a through March 2005. Every fourth 1-km MODIS pixel and every other scan line are sampled to minimize processing time and data storage. The SSF consists of the cloud properties, imager radiances, and other parameters convolved with the CERES scanner point spread function into the each CERES footprint to effect an optimal match between the cloud and radiation parameters.

Each MODIS pixel is initially classified as clear or cloudy using updated versions of the CERES classification schemes that employ the 0.64 (visible), 1.6 or 2.1 (near infrared), 3.7 (solar infrared), 10.8 (infrared), and 12 (split window) μm radiances (Trepte et al., 1999, 2002). The 1.6-μm channel is used as the near-infrared data from VIRS and *Terra*, while the 2.1-μm channel is used for *Aqua* because of problems with

the *Aqua* 1.6-μm channel. To detect cloudy pixels, the radiances are compared with predicted clear-sky radiances based on empirical estimates of spectral clear-sky albedo (Sun-Mack et al., 1999, 2003) and on skin temperatures from the CERES Meteorology, Ozone, and Aerosol (MOA) dataset adjusted using empirical estimates of spectral surface emissivity (Chen et al., 2002) and atmospheric absorption calculated with the MOA vertical profiles of temperature and humidity. The CERES MOA profiles are based on the European Center for Medium-range Weather Forecasting (ECMWF) reanalyses for VIRS and on the Global Modeling Assimilation Office GEOS 4.03 (DAO, 1997) reanalyses for *Terra* Edition 2a and *Aqua* Edition 1. The differences between the 1.6- and 2.1-μm reflectances for clear snow surfaces necessitated some adjustments to the cloud mask algorithms that are described by Minnis et al. (2003).

Effective droplet radius r_e or effective ice crystal diameter D_e, *OD*, water path *WP,* cloud temperature T_c, height z_c, thickness, and cloud phase are derived from these same radiances using one of three different techniques. The visible infrared solar-infrared split-window technique (VISST), an updated version of the 3-channel daytime method of Minnis et al. (1995), is used during daytime, which is defined as the time when the solar zenith angle *SZA* is less than 82°. At other times of day, the solar-infrared infrared split-window technique (SIST) is used to determine all of the parameters. The SIST, an improved version of the 3-channel nighttime method of Minnis et al. (1995), only uses thermal and solar infrared data. Thus, its retrievals are valid only for optically thin clouds. When the SIST is used, default values are used for all parameters except phase, T_c, and z_c for clouds with $OD < 8$. The third method, developed by Platnick et al. (2001), is designated the solar-infrared infrared near-infrared technique (SINT) and is only applied to MODIS data during the daytime for clouds over snow or ice backgrounds. The 2.13-μm channel on *Aqua* is used instead of the 1.6-μm channel in the SINT. Determination of the background surface as snow or ice can either come from the scene classification for adjacent clear pixels or from the snow and ice maps used in the CERES data stream (Trepte et al., 2002). All of the methods compute both ice and liquid water solutions that simultaneously determine T_c, *OD*, and particle size. Each method iteratively matches the observed radiances to TOA radiances calculated using emittance and reflectance parameterizations that account for atmospheric attenuation and surface reflectance and emission. The cloud reflectances and emittances are included in the parameterizations (Minnis et al., 1998, Arduini et al., 2002) using updated lookup tables for each specific channel. The phase is selected for each pixel based on the cloud temperatures, the availability of a solution, best consistency with a solution, and the altitude of the cloud.

To provide the link between clouds and the radiation budget, the pixel-level data are convolved with the individual broadband CERES radiative fluxes. These SSF products include the cloud fraction and mean associated properties for up to two cloud layers. No cloud properties could be retrieved for ~6.7% of pixels classified as cloudy during the daytime. At night, only 1.4% of the cloudy pixels are inconsistent with the parameterizations. Most of the no-retrieval pixels occur in polar regions over snow-covered surfaces or over very bright deserts. In the former instance, the SINT is unable to find a match, probably because of uncertainties in the clear-sky reflectance fields. In the latter case, the pixels detected as clouds may actually be heavy concentrations of aerosols that are misclassified as clouds. Over most ocean and land areas outside the polar regions and Saharan Desert, the no-retrievals account for 1 - 2% of the total number of cloudy pixels. To account for the no-retrievals, the SSF convolution assigns the mean cloud properties from cloudy pixels in the footprint with retrieved values to the no-retrieval pixels, if more than 1/9 of pixels in the footprint have valid cloud retrievals. Otherwise, only the valid cloudy pixels are used and the no-retrieval pixels are not considered as part of the total number of pixels in the footprint.

Edition-2 VIRS cloud products are currently available for January 1998 - July 2001, but the CERES fluxes are only available for January - August 1998 and March 2000. As of this writing, the CERES Edition-2 *Terra* cloud properties have been completed for the period March 2000 through June 2005. Edition-1 *Aqua* products have been produced for July 2002 - March 2005.

3. RESULTS AND DISCUSSION

The 5-year time series of monthly mean cloud amounts from Terra are plotted in Fig. 1 and Fig. 2, for 5 different latitude zones, where Fig. 1 is for liquid water clouds over land and Fig. 2 is for ice clouds. These results represent the daytime retrieval (nighttime results are not shown). In this paper, the seasons are defined relative to the Northern Hemisphere with winter defined by December, January, and February. The 5 latitude zones are defined as Northern Hemisphere Polar (NHP, 60°N - 90°N), Northern Hemisphere (NH) Midlatitude (NHM, 30°N - 60°N), Tropics (TP: 30°S - 30°N), Southern Hemisphere (SH) Midlatitude (SHM, 30°S - 60°S), and Southern Hemisphere Polar (SHP, 60°S - 90°S). Liquid water clouds (Fig. 1a) are most prevalent in the NH during summer and, conversely, are found least often in the SH during the same season except over the SHP. It appears that SHP zone has the most cloud cover during spring and the least during fall. The movement of the Intertropical Convergence Zone (ITCZ) is evident in the shift from maximum cloud cover during the summer and fall to a minimum during the winter for all zones except in the SHP zone. The seasonal cycle results from changing temperature patterns and, in some part, to the variations in ice cloud cover that can block the satellite view of underlying water clouds. For

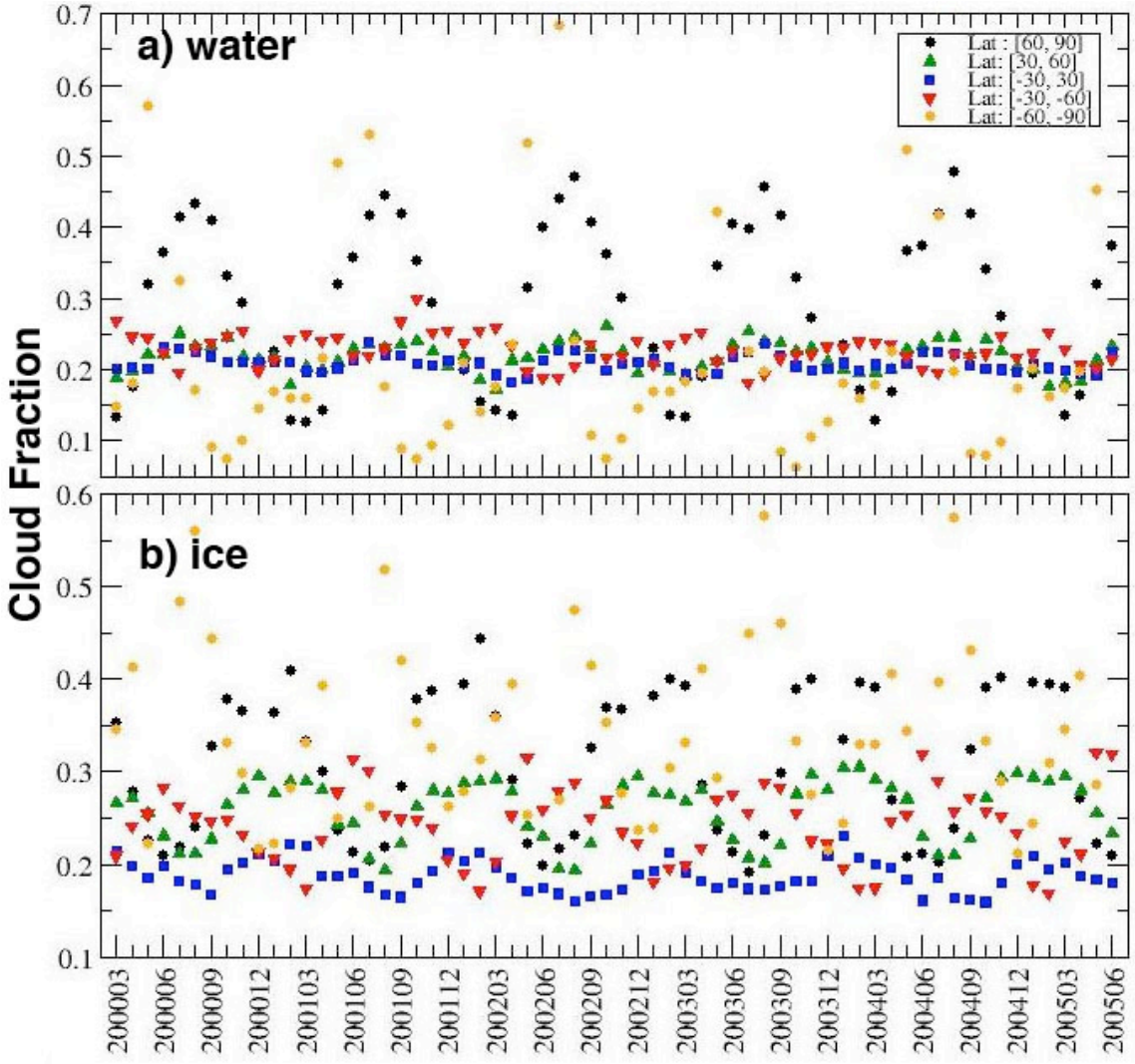

Fig. 1. *Monthly mean daytime cloud cover over land, from CERES Terra MODIS analyses, March 2000 - June 2000.*

example, the maximum in ice cloud cover (Fig. 1b) coincides with the minimum in liquid water clouds during the Northern Hemisphere winter and vice versa during the summer. Multilayer cloud detection methods and a deeper analysis of surface data would be needed to determine if the liquid cloud cover actually decreases during winter or if it is simply taken out of view by the ice clouds. The water cloud coverage over ocean (not shown) varies more with season than over land, except in the Arctic and Antarctica. Ice cloud amounts shift latitudinally with season producing a minimum during summer in the Northern Hemisphere and maxima during winter. Ice cloud amount for polar zones is rather noisy and more so for SHP zone (Fig. 1b). This is probably due to the errors in CERES mask and CERES cloud phase retrieval. Reliably detecting clouds is extremely difficult in the cold, low thermal contrast conditions of the polar regions like Antarctica.

The general patterns in the cloud amount for both *Aqua* and *Terra* are very similar for both satellites with *Aqua* being less cloudy for liquid water cloud over ocean (not shown). The regions dominated by low-level marine stratocumulus clouds have less cloudiness at 1330 LT compared to that at 1030 LT. Over ocean and many areas with deep convection, the cloud cover is greater at 1330 LT than during the midmorning (not shown). These diurnal variations are consistent with climatology.

The annual mean cloud amounts computed from the seasonal averages are plotted in Fig. 2 with the zonal mean cloud amounts derived from all available surface observations for the 1971-1996 period and with zonal averages from ISCCP for 1983-2001. All three CERES (*Aqua*-MODIS, *Terra*-MODIS and TRMM-VIRS) total cloud amounts track the surface values except *Terra* in Antarctica where the CERES *Terra* values are 5 - 20% more than the surface means. However, three other datasets (CERES Aqua-MODIS, surface, and ISCCP) agree exceptionally well near the South Pole. Other differences are evident in the Arctic where both CERES *Aqua* and *Terra* cloud amounts are 3 - 20% less than the surface and ISCCP averages The differences are primarily due to underestimates during the polar

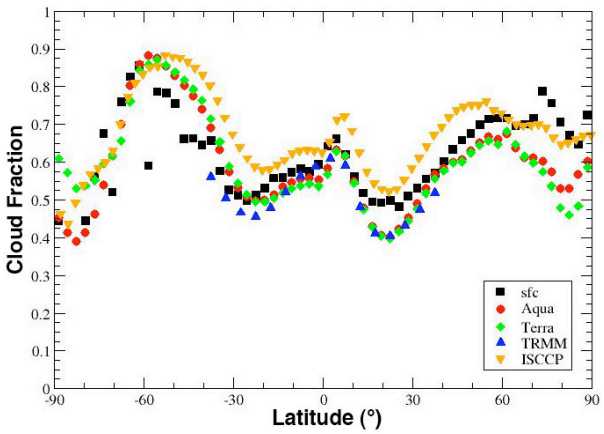

Fig. 2. *Mean total cloud cover from surface (sfc) observations (1971-1996), CERES Terra MODIS (2000-2005), CERES Aqua MODIS (2002-2005), CERES TRMM VIRS (1998-2001), and ISCCP (1983-2001).*

night (Uttal et al., 2005). The surface and ISCCP means are larger than their CERES counterparts for all latitudes north of 30°S. The CERES averages are slightly larger in the southern midlatitudes and over the South Pole. Despite substantial zonal differences between the five datasets, the annual mean global cloud cover from the surface, CERES *Aqua*-MODIS, CERES *Terra*-MODIS, and ISCCP, are quite close with values of 0.614, 0.592, 0.595, 0.504, and 0.666, respectively. Between 37.5° and 37.5°S, the respective mean annual cloud amounts are 0.554, 0.545, 0.538, and 0.628 compared to 0.504 from the VIRS.

The time series of monthly mean daytime effective cloud height from *Terra* over ocean are plotted in Fig. 3. Seasonal variations in cloud height over ocean for the period of record show the seasonal shift of the ITCZ. The seasonal variations of liquid water cloud height (Fig. 3a) for the NHP, SHP and NHM zones are much larger (up to 1 km) than the SHM and TP zones (up to 250 m). Mean liquid water cloud heights under the marine subtropical high pressure system are generally less than 2.5 km. Over the Arctic Ocean and the seas surrounding Antarctica, the water cloud height varies between 1 and 2.5 km, heights consistent with the predominance of stratus, altostratus, and nimbostratus in those area (Warren et al., 1988). Increases in the average heights of water clouds for NHM zone occur in winter and decrease in summer. Ice cloud height for the same zone varies in the opposite fashion (Fig. 3b). Ice cloud heights over ocean for the TP zone are well separated from and much higher, at 9.8 km, than over the other zones, about 9.8 km. The seasonal variation for all zones, except the TP zone, is about 2-3 km.

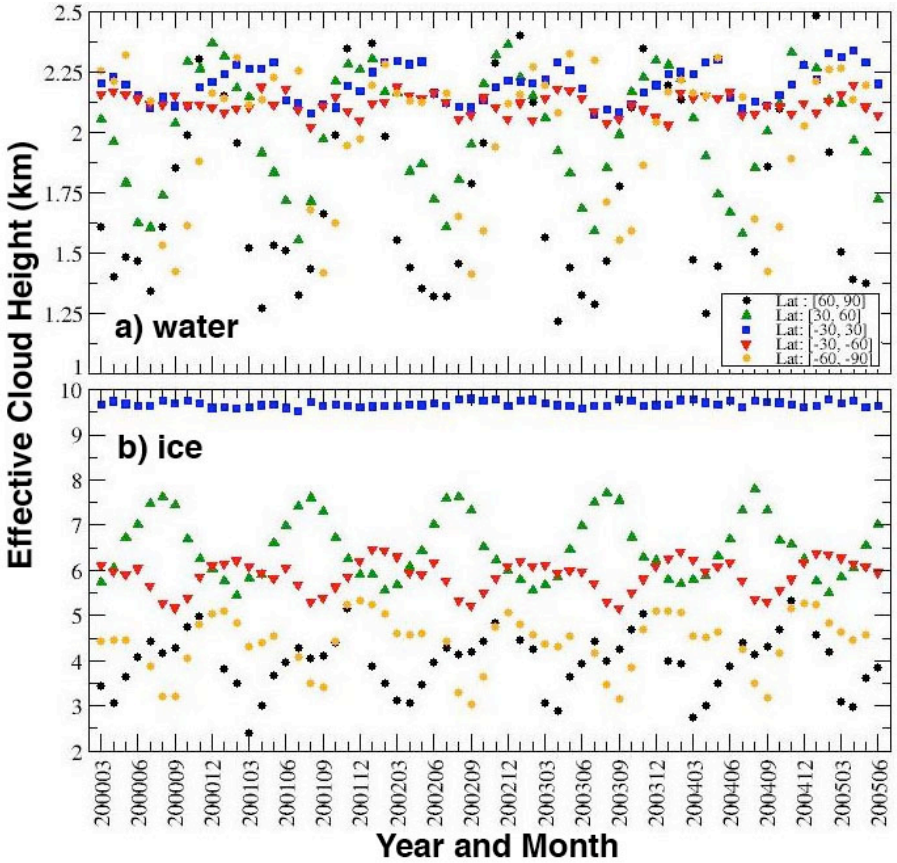

Fig. 3. *Monthly mean daytime cloud height over ocean from CERES Terra MODIS analyses, March 2000 - June 2005.*

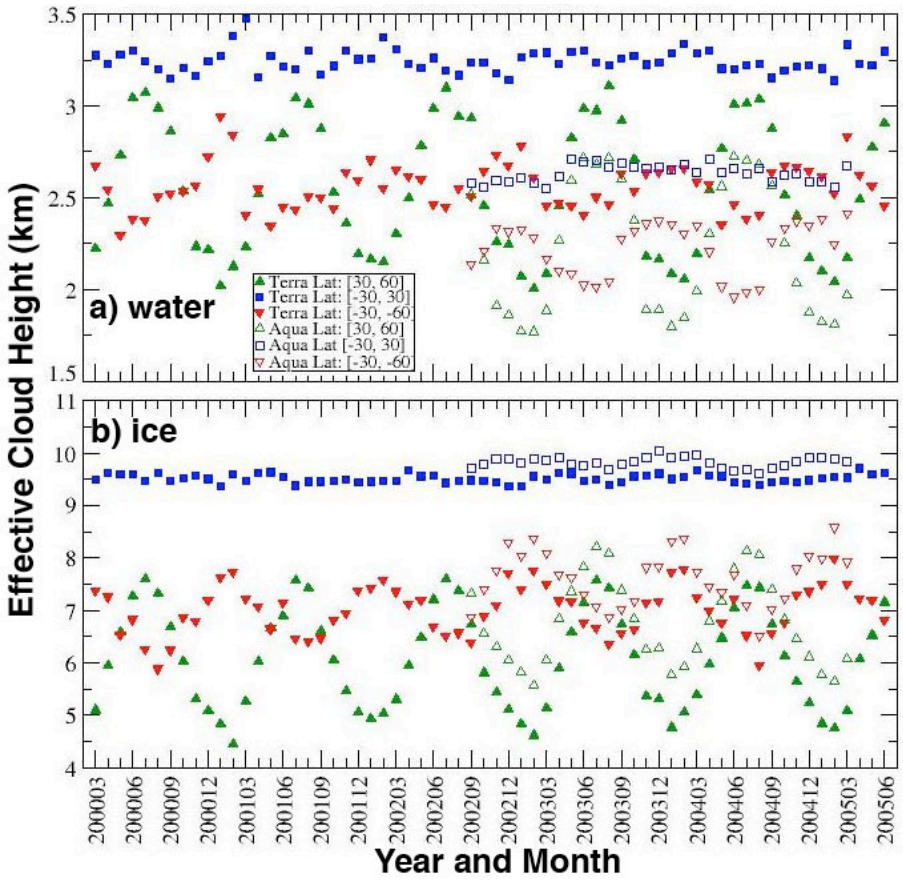

Fig. 5. *Monthly mean daytime cloud effective height cloud over non-polar land from CERES Terra and Aqua MODIS analyses.*

The time series of cloud heights over land from *Aqua* and *Terra* are shown in Fig. 5. The regions dominated by low-level clouds over land or desert areas having more cloudiness at 1330 LT have lower liquid water cloud heights (Fig. 5a) than those at 1030 LT. The diurnal water cloud height differences range from 0.5 km to 1 km for the zones shown, and almost no differences were found for the polar regions (not shown). The opposite effect can be seen for ice cloud height (Fig. 5b), where the *Aqua* cloud heights track their *Terra* counterparts closely with *Aqua* ice clouds about 0.5 km higher than those from *Terra*. Over the deserts of North Africa and southwestern Asia, the cloud amounts are slightly greater during the afternoon. Ice cloud heights over those deserts are generally around 8 km, on average, consistent with the predominance of the cirrus and altocumulus cloud types there (Warren et al., 1986). Ice cloud height is also higher at 1330 LT than during midmorning for the two polar zones (not shown) with noisier monthly means than for the three non-polar zones.

The distributions of linearly averaged liquid cloud optical depth for the 2 example months are shown Fig. 6. The average values for the stratocumulus clouds in the subtropical high areas are around 10, while the trade cumulus cloud *OD* ranges from 3 to 8. The stratus clouds in the NH storm tracks during January have the largest optical depths averaging between 16 and 32. The thickest water clouds are found at similar latitudes

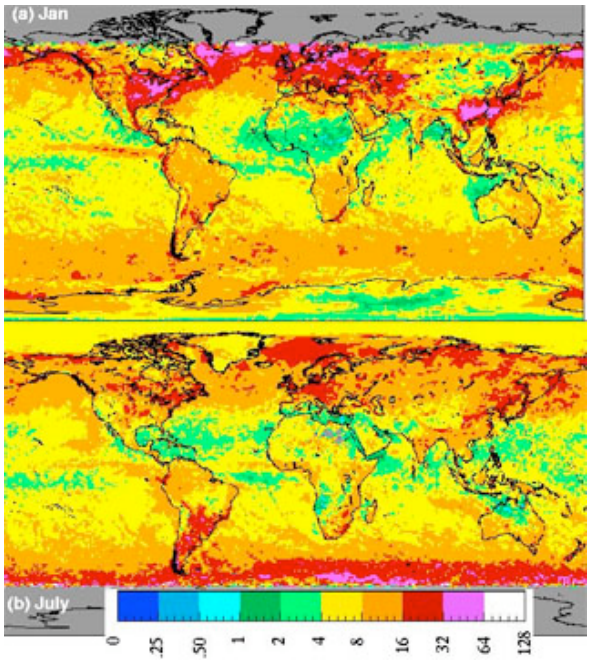

Fig. 6. Mean water cloud optical depth from CERES Aqua data, January 2005 and July 2004.

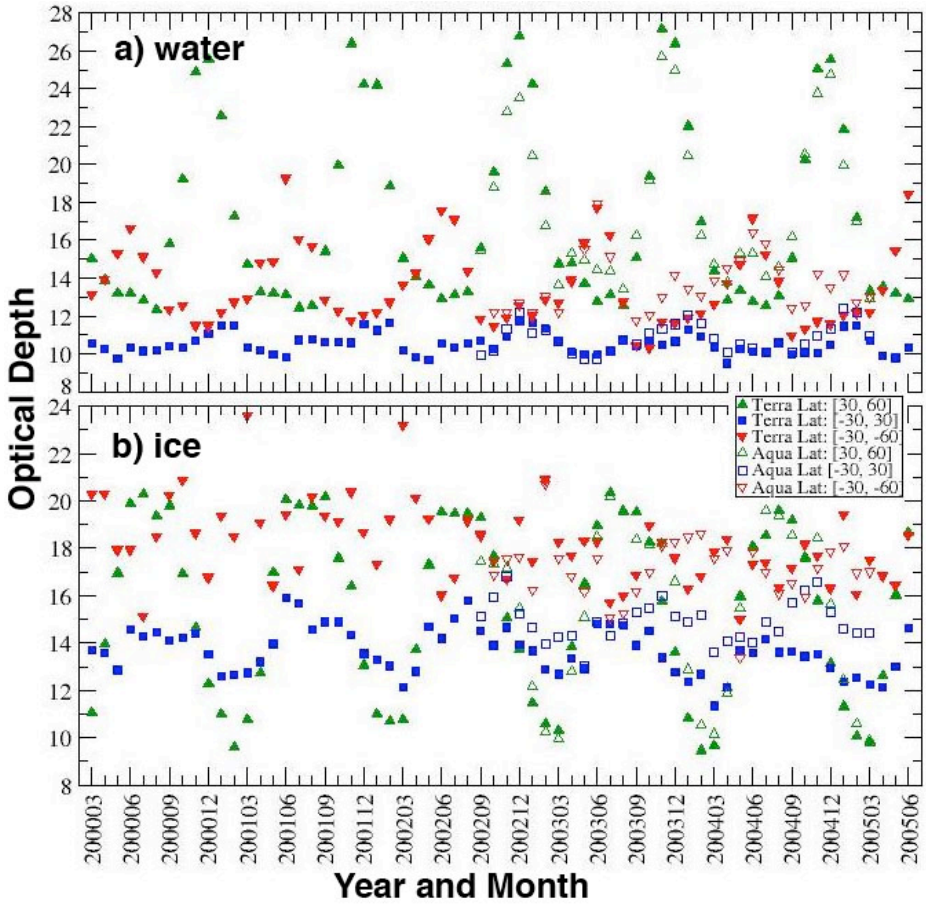

Fig. 7. *Same as Fig. 5, except for cloud optical depth.*

in the SH during July. This seasonal switch in *OD* is more readily seen in Fig. 7, which shows the seasonal variability in water (Fig. 7a) and ice cloud (Fig. 7b) *OD* for non-polar land areas for *Terra* and *Aqua*. The largest water cloud OD and smallest ice cloud OD occur during the NH winter . This behavior reverses during the NH summer. The SHM is noisier because of the lack of land samples compared with other latitude zones. The ice *OD* in land polar regions (not shown) decreases during non-summer seasons and the water OD increases in the NHP zone. This behavior may be related to the use of the SINT over snow-covered surfaces. Because the method has not been examined in depth yet, it cannot be concluded whether the drop is an artifact or an actual decrease in *OD*. The afternoon liquid water clouds (*Aqua* 1330 LT) are slightly thinner than the morning clouds (*Terra* 1030 LT). There are almost no diurnal differences in ice cloud OD for the NH zones (Fig. 7b) between 1030 LT and 1330 LT for all seasons, except fall when the afternoon clouds are thicker.

Figure 8 shows the mean cloud water droplet radius distribution for January 2005 and July 2004 from *Aqua*. The values of r_e are smallest over land and desert areas. Over water, r_e is least near coastal areas and greatest over open ocean. During January, strong westerly flow off the North American and Asian coasts is probably responsible for the smaller values of r_e east of those continents while an increase in burning over

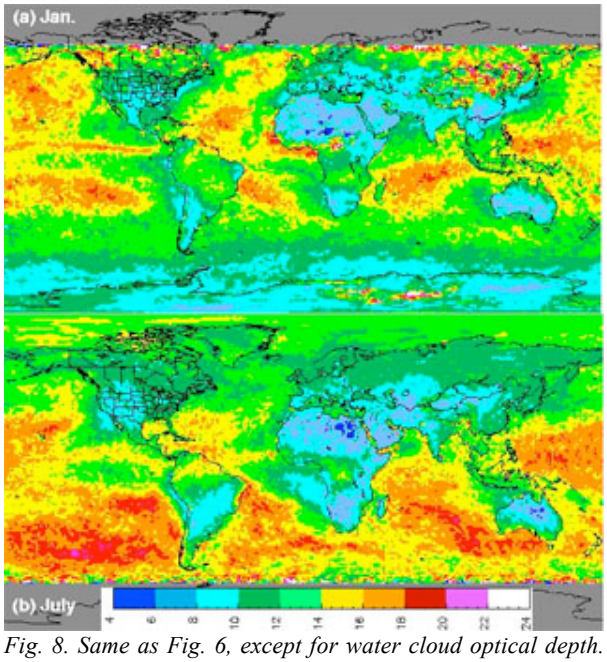

Fig. 8. Same as Fig. 6, except for water cloud optical depth.

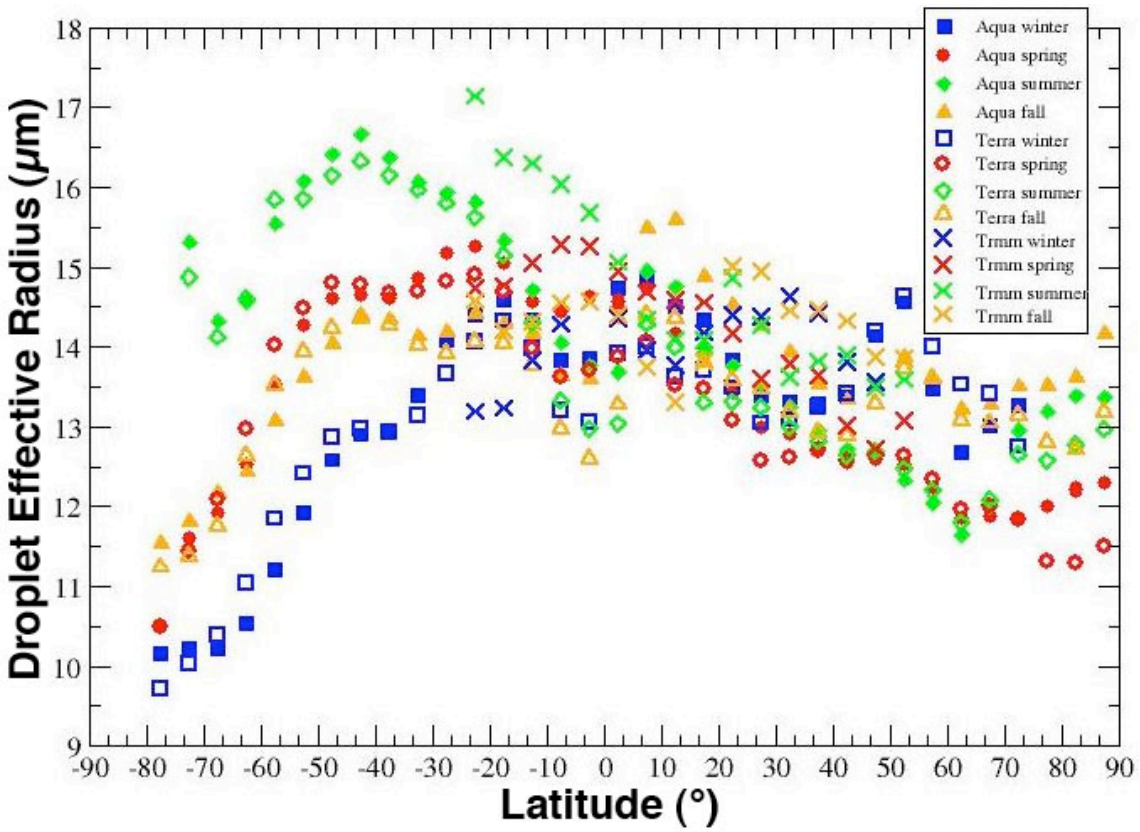

Fig. 9. *Seasonal variation in r_e over ocean from Aqua MODIS (solid) 2002-2005, Terra MODIS (open) 2000-2005, and VIRS (X), 1998-2001. NH winter (blue), spring (red), summer (green), and fall (gold).*

southern Africa during July may be the source of the decreased r_e over the South Atlantic. Similar burning over South America may also help reduce r_e over Brazil during July. The very large values of r_e over the oceans are probably linked to drizzling clouds in those pristine areas. The even greater values near the terminator lines are likely due to ice contamination or to the effects of lower sun angles and shadowing.

The seasonal variations in zonal mean r_e in Fig. 9 for ocean areas. Maximum values of r_e occur in the SH during the boreal summer over all surfaces (land not shown). The maximum variations are also found in the SH. Variations in the Tropics are relatively small for r_e and D_e (not shown) over all surfaces. The mean effective radius changes very little with season, except for winter, over NH land (not shown), but over ocean it varies 2 μm with a peak during fall and winter and a maximum during summer. The mean value of D_e in the Tropics over land is around 45 μm compared to approximately 51 μm over water.

The SZA varies seasonally with latitude and might be related to the extreme seasonal variation in r_e over the SH oceans even though preliminary analyses indicate very little dependence of r_e on SZA (Heck et al., 2002). If anything, it decreases slightly with increasing SZA. The VIRS samples all available SZAs for a given zone during a season and should cover the same range of SZA in a given latitude belt in both hemispheres. If the variations are due to angular effects, then the NH and SH should produce the same type of seasonal variability. Figure 18 shows that the VIRS and MODIS data produce similar zonal patterns of mean r_e and that the extreme variation in r_e over the SH is probably due to some other effect, which is probably related to the availability of more cloud condensation nuclei during the austral summer. Determining why this variability occurs should greatly advance our understanding of cloud processes and the natural production of aerosols.

There are many more parameters that could be examined. However, a complete analysis of the CERES cloud dataset is beyond the scope of this paper.

4. CONCLUDING REMARKS

This paper has presented a brief summary of 5 years of cloud properties derived from *Terra* MODIS data and 3 years from *Aqua* MODIS for CERES. The results are consistent between satellites and with surface measurements, in general, with some exceptions in the Arctic. Much more validation work remains but the data are already proving valuable for radiation budget studies and should be especially useful for studying cloud and aerosol interactions and

performing climate model validations. The data are publicly available at the NASA Langley Research Center Distributed Active Archive. Additional data from *Terra* and *Aqua* will be archived as data processing continues. Shortcomings in the datasets will be addressed in future editions of the analyses.

ACKNOWLEDGEMENTS

This research was supported by the NASA Science Directorate through the CERES Project.

REFERENCES

Arduini, R. F., P. Minnis, and D. F. Young, 2002: Investigation of a visible reflectance parameterization for determining cloud properties in multi-layered clouds. *Proc. 11th AMS Conf. Cloud Physics*., Ogden, UT, June 3-7, CD-ROM, P2.4.

Chen, Y., S. Sun-Mack, P. Minnis, D. F. Young, and W. L. Smith, Jr., 2002: Surface spectral emissivity derived from MODIS data. *Proc. SPIE 3rd Intl. Asia-Pacific Environ. Remote Sensing Symp.: Remote Sens. of Atmos., Ocean, Environment, and Space*, Hangzhou, China, October 23-27, **4891**, 361-369.

DAO, 1997: GEOS-3 Data Assimilation System Architectural Design. *DAO Office Note 97-06*. Data Assimilation Office, Goddard Space Flight Center, Greenbelt, MD 20771.

Hahn, C. J., and S. G. Warren, 1999: *Extended Edited Synoptic Cloud Reports from Ships and Land Stations Over the Globe, 1952-1996*. NDP026C, Carbon Dioxide Information Analysis Center, Oak Ridge National Laboratory, Oak Ridge, TN.

Heck, P. W., P. Minnis, D. F. Young, and S. Sun-Mack, 2002: Angular variations of cloud properties from VIRS and MODIS data. *Proc. 11th AMS Conf. Atmos. Rad*., Ogden, UT, June 3-7, 148-151.

Huang, J., P. Minnis, B. Lin, Y. Yi, M. M. Khaiyer, R. F. Arduini, and G. G. Mace, 2004: Advanced retrievals of multilayered cloud properties using multi-sensor and multi-spectral measurements. Accepted, *J. Geophys. Res*., 10.1029/2004JD005101.

Loeb, N. G., N. Manalo-Smith, S. Kato, W. F. Miller, S. Gupta, P. Minnis, and B. A. Wielicki, 2003: Angular distribution models for top-of-atmosphere radiative flux estimation from the Clouds and the Earth's Radiant Energy System instrument on the Tropical Rainfall Measuring Mission satellite. Part I: Methodology. *J. Appl. Meteorol*., **42**, 240-265.

Minnis, P., D. P. Garber, D. F. Young, R. F. Arduini, and Y. Takano, 1998: Parameterization of reflectance and effective emittance for satellite remote sensing of cloud properties. *J. Atmos. Sci*., **55**, 3313-3339.

Minnis, P., et al., 1995: Cloud Optical Property Retrieval (Subsystem 4.3). "Clouds and the Earth's Radiant Energy System (CERES) Algorithm Theoretical Basis Document, Volume III: Cloud Analyses and Radiance Inversions (Subsystem 4)", *NASA RP 1376 Vol. 3*, pp. 135-176.

Minnis, P., D. F. Young, S. Sun-Mack, P. W. Heck, D. R. Doelling, and Q. Z. Trepte, 2003: CERES cloud property retrievals from imagers on TRMM, Terra, and Aqua. *SPIE 10th Intl. Symp Remote Sens., Conf. Remote Sens. Clouds and Atmos*., Barcelona, Spain, September 8-12, 37-48.

Minnis, P., D. F. Young, B. A. Weilicki, S. Sun-Mack, Q. Z. Trepte, Y. Chen, P. W. Heck, and X. Dong, 2002: A global cloud database from VIRS and MODIS for CERES. *Proc. SPIE 3rd Intl. Asia-Pacific Environ. Remote Sensing Symp. 2002: Remote Sens. of Atmosphere, Ocean, Environment, and Space*, Hangzhou, China, October 23-27, Vol. 4891, 115-126.

Pallé, E., P. R. Goode, P. Montañés-Rodríguez, and S. E. Koonin, 2004: Changes in Earth's reflectance over the past two decades. *Science*, **304**, 1299-1301

Platnick, S., J. Y. Li, M. D. King, H. Gerber, and P. V. Hobbs, A solar reflectance method for retrieving cloud optical thickness and droplet size over snow and ice surfaces. *J. Geophys. Res*., **106**, 15185-15199, 2001.

Rossow, W. B. and R. A. Schiffer, 1999: Advances in understanding clouds from ISCCP. *Bull Am. Meteor. Soc*., **80**, 2261-2287.

Spangenberg, D. A., Q. Trepte, P. Minnis, and T. Uttal, 2004: Daytime cloud property retrievals over the Arctic from multispectral MODIS data. *Proc. 13th AMS Conf. Satellite Oceanogr. and Meteorol*., Norfolk, VA, Sept. 20-24, CD-ROM, P7.11.

Sun-Mack, S., Y. Chen, T. D. Murray, P. Minnis, and D. F. Young, 1999: Visible clear-sky and near-infrared surface albedos derived from VIRS for CERES. *Proc. AMS 10th Conf. Atmos. Rad*., Madison, WI, June 28 – July 2, 422-425.

Sun-Mack, S., P. Minnis, Y. Chen, and R. F. Arduini, 2003: Clear-sky narrowband albedos derived from VIRS and MODIS. *SPIE 10th Intl. Symp Remote Sens., Conf. Remote Sens. Clouds and Atmos*., Barcelona, Spain, September 8-12, 101-109.

Trepte, Q., Y. Chen, S. Sun-Mack, P. Minnis, D. F. Young, B. A. Baum, and P. W. Heck, 1999: Scene identification for the CERES cloud analysis subsystem. *Proc. AMS 10th Conf. Atmos. Rad*., Madison, WI, June 28 – July 2, 169-172.

Trepte, Q., P. Minnis, and R. F. Arduini, 2002: Daytime and nighttime polar cloud and snow identification using MODIS data. *Proc. SPIE 3rd Intl. Asia-Pacific Environ. Remote Sensing Symp. 2002: Remote Sens. of Atmosphere, Ocean, Environment, and Space*, Hangzhou, China, October 23-27, Vol. 4891, 449-459.

Uttal, T., S. Frisch, X. Wang, J. Key, A. Schweiger, S. Sun-Mack, and P. Minnis, 2005: Comparison of monthly mean cloud fraction and cloud optical depth determined from surface cloud radar, TOVS, AVHRR, and MODIS over Barrow, Alaska. *Proc. AMS 8th Conf. Polar Meteorol*., San Diego, CA, January 9-13, CD-ROM, P1.27.

Warren, S. G., C. J. Hahn, J. London, R. M. Chervin, and R. L. Jenne, Global distribution of total clouf

cover and cloud type amounts over ocean, NCAR Tech. Note NCAR/TN-317+STR, 212 pp.,1988.

Warren, S. G., C. J. Hahn, J. London, R. M. Chervin, and R. L. Jenne, Global distribution of total clouf cover and cloud type amounts over ocean, NCAR Tech. Note NCAR/TN-273+STR, 229 pp.,1986.

Wielicki, B. A., et al., 1998: Clouds and the Earth's Radiant Energy System (CERES): Algorithm overview. *IEEE Trans. Geosci. Remote Sens.*, **36**, 1127-1141.

Wielicki, B. A., T. Wong, N. Loeb, P. Minnis, K. Priestley, and R. Kandel, 2005: Changes in Earth's albedo measured by satellites. *Science*, **308**, 825.